Enhanced Photoelectrocatalytic Activity of FTO/WO_3/$BiVO_4$ Electrode by Modified With Gold Nanoparticles for Water Oxidation Under Visible Light Irradiation

Ponchio Chatchai, Shin-ya Kishioka[1], Yoshinori Murakami, Atsuko Y. Nosaka, and Yoshio Nosaka*,[1]

Department of Chemistry, Nagaoka University of Technology, Nagaoka, 940-2188 Japan

Received Month XX, 200X; Accepted Month XX, 200X

* E-mail: *nosaka@nagaokaut.ac.jp*
Tel/Fax: +81-258-47-9315

[1] ISE member

Abstract

Gold nanoparticles were successfully deposited on FTO/WO_3/$BiVO_4$ electrode surface by means of electrolysis of $AuCl_4^-$ ions. The composite films were characterized by SEM, XPS and XRD techniques. An increase in photocurrent and a negative shift of onset potential for water oxidation were observed upon modification of the electrode surface with the Au particles. The electrochemical impedance spectroscopy was used to confirm the acceleration of charge transfer process by Au deposition at the electrode surface. The photocurrent action spectrum did not correlate with the plasmonic absorbance of Au nanoparticles at 560 nm, suggesting that the Au nanoparticles increased charge separation without undergoing a plasmon resonance effect under visible light irradiation.

Keyword: coupled WO_3/$BiVO_4$, gold nanopaticles, composite electrode, photoelectrocatalyst, water oxidation

1. Introduction

The photocatalytic water oxidation driven by visible light irradiation is one of the most attractive targets concerning with the development of oxygen evolution as a coupled reaction to the hydrogen production of solar water splitting. Many oxide semiconductors such as $BiVO_4$, WO_3, Co_3O_4, Fe_2O_3 [1-5] and so on have been used as a photocatalyst with absorption ability in visible light region. Among them, $BiVO_4$ showed the highest activity for water oxidation [6]. However, the photocatalytic activity of $BiVO_4$ alone is low due to the recombination between photoinduced electrons at the conduction band and photoinduced holes at the valence band. The coupled semiconductor or semiconductor composites could enhance the photocatalytic activity by rapid removing of the photoinduced electrons form conduction band [7-9].

Our work has been projected to develop the photocatalytic activities of $BiVO_4$ electrode by coupling with SnO_2 [10]. The photocurrent of $BiVO_4$ electrode increased when SnO_2 was deposited between the layers of $BiVO_4$ and an F-doped tin oxide (FTO) conducting electrode. Recently, we have reported that a composite $WO_3/BiVO_4$ film electrode has higher photocurrent efficiency than the coupled $SnO_2/BiVO_4$ because the WO_3 has a more suitable energy band level than SnO_2 for efficient charge separation [11]. We have also revealed that the sequence of the composite fabrication is an important factor for the high photocatalytic activity. However, the photocatalytic activity of these composite electrodes is required to be improved in visible light region for practical use.

Noble metal nanoparticles, especially gold (Au) particles have been interesting because it could enhance the visible light absorption based on surface plasmon resonance effect and play as catalysts for interfacial charge-transfer process [12-14]. Therefore, the combination of gold nanoparticles and coupled $WO_3/BiVO_4$ electrodes was expected to promote the photocatalytic

activity of FTO/WO_3/$BiVO_4$ electrodes. In this work, the nanoparticles of Au were deposited on an FTO/WO_3/$BiVO_4$ electrode by the electrodeposition technique and a significant enhancement of the photocatalytic properties for water oxidation under visible light irradiation will be reported.

2. Experimental

2.1 Preparation of the FTO/WO_3/$BiVO_4$ film photoelectrode

Precursor solutions of 0.05 M (M = mol dm^{-3}) $BiVO_4$ and 0.10 M WO_3 were prepared as described previously [11]. FTO/WO_3/$BiVO_4$ film electrodes were fabricated by the deposition of a WO_3 layer on an FTO conducting electrode followed by the deposition of a $BiVO_4$ layer on the surface of the WO_3 layer. For the deposition, the precursor solutions were coated by means of a spin coater (1,000 rpm, 40 sec.) on an FTO substrate (40 mm x 20 mm), and then dried at 150°C for 5 min for every coating. After the coatings, every sample was calcined at 550°C for 1 hour in air. The edges of the electrodes were covered with epoxy resin to confine the irradiation area to 1 cm^2. The number of coatings, which was first selected to obtain the highest photocatalytic activity, was 5 times for $BiVO_4$ layer and once for WO_3 layer. The thickness of the $BiVO_4$ layer was about 1 μm [10, 11].

2.2 Preparation of FTO/WO_3/$BiVO_4$/Au electrode

Gold nanoparticles were electrodeposited onto the FTO/WO_3/$BiVO_4$ electrode according to the literature [15] by the following procedure. Constant potential at -0.1 V (vs Ag/AgCl) was applied for 10 to 480 s in 0.1M KNO_3 electrolyte solution containing 0.1%(w/v) $HAuCl_4$. After the deposition the electrode was washed with pure water and dried at 150°C for 4 hours. The deposition time was typically 60 s as the optimized condition to show the highest photocurrent.

2.3 Photoelectrochemical measurements and characterization

The optical absorption spectra of the composite electrodes were measured by using a UV/Vis spectrophotometer (Shimadzu, UV-3150). The recorded absorption spectra were corrected for the interference by the transmission modulation simulated with a single sinusoidal function. The morphology of electrode surface was studied by using a scanning electron microscope (SEM), (Technex Co., Tiny-SEM 1710) after the glass substrates were cut and coated with Au. X-ray photoelectron spectroscopy (XPS) measurements were carried out using a JPS-9010TR (JEOL) spectrometer with a monochromatic MgKα source. X-ray diffraction (XRD) patterns were recorded with a diffractometer (MAC Science, M03HF22) using CuKα radiation.

Photocurrent was measured by a three-electrode system, where a Pt wire was the counter electrode, an Ag/AgCl was the reference electrode and the prepared composite electrodes were served as the working electrode. An aqueous solution of 0.5 M Na_2SO_4 was used as the electrolyte. A voltammetry analyzer (Hokuto Denko, HSV-100) was used in the measurements of cyclic voltammetry and linear scan voltammetry. For the visible light irradiation at wavelength range longer than 420 nm, a 50-W tungsten lamp (Moritex, MHF-C50LR) was used with inserting an optical glass filter (Hoya, L-42) to measure the photocurrent properties. For the measurements of incident photon to current conversion efficiency, %IPCE, at each wavelength of λ, a 500 W xenon lamp (Ushio Denki Co. X500) was used as a light source and the wavelength was selected with a monochromator. Photon flux was measured by an optical power meter (Advantest Co., TQ8210). The %IPCE at each wavelength was calculated as described previously [11]. The electrochemical impedance spectroscopy (EIS) was performed with a Versa

STAT 3 (Princeton Applied Research, Inc.) under the open circuit potential at frequencies ranging from 100 kHz to 0.1 Hz under visible light ($\lambda > 420$ nm) irradiation.

3. Results and Discussion

3.1 Characterization of the film photocatalysts

Figure 1 shows the absorption spectra of the FTO/WO_3/$BiVO_4$/Au and FTO/WO_3/$BiVO_4$ electrodes. The absorption edges of the spectra for both electrodes were approximated to 510 nm, which corresponds to the band gap energies of ca. 2.43 eV [16]. This value is consistent with the band gap energy of $BiVO_4$ (2.4 eV) [11]. The FTO/WO_3/$BiVO_4$/Au electrode showed the absorption at around 560 nm, corresponding to the surface plasmon resonance band of Au nanoparticles [17-19]. This indicates that Au nanoparticles have been assembled successfully on the FTO/WO_3/$BiVO_4$ electrode to show the enhanced visible absorption owing to the surface plasmon resonance.

The SEM images of the electrode surfaces (Figure 2) showed that the particle size of Au ranged from 50 to 100 nm and smaller than that of the surface grains of WO_3/$BiVO_4$. The surface morphology was different from those deposited by the vacuum evaporation and sputtering methods. This result indicates that electrodeposition is favorable to prepare Au nanoparticles with a high surface-area size on FTO/WO_3/$BiVO_4$ electrode.

X-ray photoelectron spectroscopy (XPS) was used to identify the chemical states of the Au on the FTO/WO_3/$BiVO_4$ surface. The shift of peak position on the charge effect was calibrated using the binding energy of C 1s at 284.8 eV [20]. In the XPS spectra, the peaks of Au $4f_{7/2}$ and $4f_{5/2}$ were located at 83.5 and 87.2 eV, respectively, which were assigned to metallic gold (Au^0) [13]. Moreover, to identify the crystalline structure of Au, the XRD patterns were

recorded before and after the Au electrodeposition on FTO/WO_3/$BiVO_4$ electrodes. As shown in Figure 3, the XRD peaks observed at 2θ = 38.2°, 44.4° and 64.5° were attributable to the diffractions of (111), (200) and (220) planes of cubic gold metal crystal [15, 21, 22], respectively. The remained XRD peaks are ascribed to the tetragonal structure of SnO_2, monoclinic sheelite of $BiVO_4$, and monoclinic WO_3 as reported previously [11]. Therefore, these XRD measurements also indicated the formation of Au, $BiVO_4$ and WO_3 on the FTO substrate.

3.2 Photoelectrochemical properties

Cyclic voltammetric technique was used to study the photocurrent properties of the FTO/WO_3/$BiVO_4$/Au electrode in a Na_2SO_4 solution under visible-light irradiation ($\lambda > 420$ nm) and compared with that of the FTO/WO_3/$BiVO_4$ electrode. As shown in Figure 4, the anodic photocurrent of the FTO/WO_3/$BiVO_4$/Au electrode was significantly enhanced as compared to that of the FTO/$BiVO_4$/WO_3 at the potential of >0.1 V (vs Ag/AgCl). Furthermore, the negative shift of the onset potential of FTO/WO_3/$BiVO_4$/Au compared to that of FTO/WO_3/$BiVO_4$ was also observed. These results indicate that the Au nanoparticles deposited on the semiconductor improved photoinduced electron transfer processes at the semiconductor interface [14, 23] and suppressed the recombination of photoinduced electron and holes. In addition to the photocurrent, dark current peaks were observed at the potentials of 1.1 V is attributable to the oxidation of Au nanoparticles. At the reverse scan shows two reduction peaks of gold oxide at 0.7 and 0.2 V (vs. Ag/AgCl) [17].

Figure 5 shows the comparison in linear scan voltammograms for the FTO/WO_3/$BiVO_4$/Au with the FTO/WO_3/$BiVO_4$ electrodes under the visible light illumination at increasing potential from 0.0 to 1.4 V. Both electrodes showed the steady increase in the anodic

photo current with applied positive potential under visible light irradiation. The FTO/WO_3/$BiVO_4$/Au electrode presents significantly higher photocurrent than the FTO/WO_3/$BiVO_4$ at the potentials ranging from 0.0 to 1.0 V. The increase in the photocurrent at a lower potential indicates that the deposition of Au nanoparticles suppress the recombination between photoinduced holes and electrons, which provide the enhancement of the charge transfer at the WO_3/$BiVO_4$ electrode surface.

An EIS measurement was applied to characterize electrochemical interfacial reaction of FTO/WO_3/$BiVO_4$/Au electrode for water oxidation under visible light irradiation. Figure 6 shows Nyquist plots for FTO/$BiVO_4$, FTO/WO_3/$BiVO_4$ and FTO/WO_3/$BiVO_4$/Au electrode in aqueous solution of Na_2SO_4. The proposed equivalent circuit consist of solution resistance (R_s), charge transfer resistance (R_{ct}) in parallel to the constant phase element (CPE) as illustrated in Figure 6. The diameter of the semicircle usually equals the R_{ct} parameter, corresponding to the efficiency of charge transfer at the electrode interface. By fitting the observed result by simulation, the R_{ct} values for FTO/$BiVO_4$, FTO/WO_3/$BiVO_4$ and FTO/WO_3/$BiVO_4$/Au electrode were obtained to be 305, 48 and 16 $k\Omega\ cm^{-2}$, respectively. This indicates that the charge transfer rate from $BiVO_4$ to FTO substrate was increased by the insertion of WO_3 layer between $BiVO_4$ and FTO. Moreover, Au at the $BiVO_4$ surface also enhances the charge transfer at the interface of the FTO/WO_3/$BiVO_4$/Au electrode and the electrolyte [24, 25].

The content of Au at electrode surface is very important factor for controlling the catalytic activity of FTO/WO_3/$BiVO_4$ electrode. Figure 7A shows the effect of the photocurrent with the content of Au at the electrodes prepared with various deposition times. The photocurrent was increased at the deposition time up to 60 s and then decreased at the longer deposition times. On the other hand, the charge transfer resistance was also increased after increased of the

deposition time more than 60 sec (Figure 7B). This experimental result represents that a small amount of Au nanoparticles deposited is suitable for enhancing the photocatalytic activity of FTO/WO_3/$BiVO_4$ electrodes. With the longer deposition time, Au will be accumulated to form particles of larger sizes and affect the active surface area of the FTO/WO_3/$BiVO_4$/Au electrode. Moreover, the thickness of Au particle layers increased and influenced the charge transfer rate at electrode surface.

The relationship between %IPCE and absorption spectrum on the wavelength of FTO/WO_3/$BiVO_4$/Au electrode is shown in Figure 8. The photocurrent action spectrum of the FTO/WO_3/$BiVO_4$/Au electrode was related to the absorption spectrum of $BiVO_4$, and did not correlate with the absorption property of Au nanoparticles. It is noteworthy that the surface plasmon absorption of the Au nanoparticles does not affect the photocurrent. This observation indicates that the plasmonic excitation of Au particles did not influence the catalytic activity at the electrode surface which acts as a catalyst.

Based on the present observations, the schematic diagram of charge transfer processes at the FTO/WO_3/$BiVO_4$/Au photo-electrodes for water oxidation under visible light irradiation is illustrated in Figure 9. Due to the matching of the energy levels, photogenerated electrons easily transfer from the conduction band of $BiVO_4$ to that of WO_3. Moreover, WO_3 layer play as the barrier for the hole of $BiVO_4$ to reach FTO surface and then decrease the recombination as described in the previous work [11]. The holes transfer at the interface between $BiVO_4$ and electrolyte is improved by the presence of Au nanoparticles deposited. Although the Au nanoparticles showed the enhancement of visible light absorption, the surface plasmon absorption did not relate with the photocurrent properties. Therefore, this improvement of photoelectrochemical performance is explained by that the Au nanoparticles act as the catalyst

for enhancing holes transfer rate from $BiVO_4$ to electrolyte [12, 14, 23, and 24]. Consequently, holes easily reach at the $BiVO_4$ surface without recombination and cause the efficient water oxidation (Figure 9A). Figure 9B shows the Au deposited on the film with particles to simplify the function of each layer. After visible light was absorbed by $BiVO_4$ layer the photogenerated electrons were separated from holes by the assistance of WO_3 layer [11]. On the other hand holes reach the $BiVO_4$/electrolyte interface to oxidize water to oxygen [26]. In this process, the small particle with high surface area of Au nanoparticles at $BiVO_4$ surface act as catalyst by enhancing the oxidation reaction with hole due to the suppression of charge recombination. Hepel et al reported that a porous WO_3 film with high surface area is beneficial to decreasing the recombination losses in bi-component WO_3/TiO_2 photoelectrode [27, 28]. Moreover, Nakato and co-workers reported that the effect of surface roughening is important for nucleophilic attack of an H_2O molecule to a surface-trapped hole of photoinduced oxygen evolution at TiO_2 surface [29], which supports our experimental result.

The modified electrodes reported in the present study provided an improved efficiency of photoinduced charge separation in a photocatalytic system. Therefore, it may be useful for other photoelectrochemical applications such as the decomposition of organic contamination in wastewater [30] and the degradation of diazo dyes in aqueous solution [31].

4. Conclusions

Spherical Au nanoparticles of cubic crystalline phase were successful fabricated by the convenient electrodeposition technique. Significant enhancement in both photocurrent and threshold photopotential for water oxidation are observed after the deposition of a small amount of Au particles on FTO/WO_3/$BiVO_4$ electrode, suggesting that charge separation was improved in the composite system. The photocurrent action spectrum was not correlated with the plasmon absorption of Au nanoparticles. The analysis of electrochemical impedance spectrum for the samples prepared with various Au deposition times indicates that Au nanoparticles act as a catalyst for enhancing the charge transfer rate at the FTO/WO_3/$BiVO_4$ electrode for water oxidation under visible light irradiation.

References

[1] A. Kudo, Int. J. Hydrogen. Energ. 32 (2007) 2673.

[2] K. Sayama, A. Nomura, H. Sugihara, J. Phys. Chem. B 110 (2006) 11352.

[3] S. K. Deb, Sol. Energ. Mat. Sol. Cells, 92 (2008) 245.

[4] M. Long, W. Cai, H. Kisch, J. Phys. Chem. C 112 (2008) 548.

[5] H. Xia, H. Zhuang, D. Xiao, Mater. Lett. 62 (2008) 1126.

[6] A. Kudo, Y. Miseki, Chem. Soc. Rev. 38 (2009) 253.

[7] S. Wang, X, Zhang, G. Cheng, Z. Du, Chem. Phys. Lett. 405 (2005) 63.

[8] M.-C. Long, R. Beranek, W.-M. Cai, H. Kisch, Electochim. Acta 53 (2008) 4621.

[9] T. Huang, X. Lin, J. Xing, F. Huang, Mat. Sci. Eng. B 141 (2007) 49.

[10] P. Chatchai, Y. Murakami, S. Kishioka, A. Y. Nosaka, Y. Nosaka, Electrochem. Solid-State Lett. 11 (2008) H160.

[11] P. Chatchai, Y. Murakami, S. Kishioka, A. Y. Nosaka, Y. Nosaka, Electochim. Acta, 54 (2009) 1147.

[12] P. V. Kamat, Pure Appl. Chem. 74 (2002) 1693.

[13] Y. Tian, T. Tatsuma, J. Am. Chem. Soc. 127 (2005) 7632.

[14] T. L. Villarreal, R. Gomez, Electrochem. Commun. 7 (2005) 1218.

[15] V. G. Praig, G. Piret, M. Manesse, S. Szunerits, Electrochim. Acta, 53 (2008) 7838.

[16] G. R. Banmwenda, K. Sayama, H. Arakawa, J. Photoch. Photobio. A, 122 (1999) 175.

[17] J. E. Park, T. Mommn, T. Osaka, Electrochim. Acta, 52 (2007) 5914.

[18] B. Ballarin, M. C. Cassani, E. Scavetta, D. Tonelli, Electrochim. Acta, 53 (2008) 8034.

[19] K. Zakrzewska, M. Radecka, A. Kruk, W. Osuch, Solid State Ionics, 157 (2003) 349.

[20] X. Cao, L. Cao, W. Yao, X. Ye, Surf. Interface Anal. 24 (1996) 662.

[21] I. Tanahashi, H. Iwagishi, G. Chang, Mater. Lett. 62 (2008) 2714.

[22] Q. He, W. Chen, S. Mukerjee, S. Chen, F. Laufek, J. Power Sources 187 (2007) 298.

[23] P. V. Kamat, Nano Lett. 3 (2003) 353.

[24] A. Dawson, P. V. Kamat. J. Phys. Chem. B 105 (2001) 960.

[25] X. Hong, L. Ling, J. Z. Yu. Chin. J. Chem. 23 (2005) 18.

[26] P. V. Kamat. Pure Appl. Chem. 74 (2002) 1693.

[27] I. Shiyanovskaya, M. Hepel. J. Electrochem. Soc. 145 (1998) 3981.

[28] I. Shiyanovskaya. M. Hepel. J. Electrochem. Soc. 146 (1999) 243.

[29] R. Nakamura, T. Okamura, Y. Nakato. J. Am. Chem. Soc. 127 (2005) 12975.

[30] X. Zhao, T. Xu, Y. Zhu. Appl. Catal. B-Environ. 72 (2007 92.

[31] M. Hepel, S. Hazelton. Electrochim. Acta, 50 (2005) 5278.

Figure Captions

Figure 1. UV-Vis absorption spectra of (a) FTO/WO_3/$BiVO_4$/Au, (b) FTO/WO_3/$BiVO_4$ and (c) FTO electrodes. The interference by the film was corrected.

Figure 2. Scanning electron micrographs (SEM) at top view of (A) FTO/WO_3/$BiVO_4$, (B) FTO/WO_3/$BiVO_4$/Au

Figure 3. The XRD patterns for the FTO, FTO/Au, FTO/WO_3/$BiVO_4$, and FTO/WO_3/$BiVO_4$/Au electrodes which are calcined under the same condition at 550^{o}C.

Figure 4. Comparison of cyclic voltammograms between FTO/WO_3/$BiVO_4$/Au and FTO/WO_3/$BiVO_4$ composite electrodes in 0.5 M Na_2SO_4 aqueous solution under the visible light illumination (> 420 nm). Scan rate was 50 mVs^{-1}. Electrolyte solution was deaerated by N_2 gas. Electrodeposition time of Au nanoparticles was 60 s.

Figure 5. Linear scan voltammograms of FTO/WO_3/$BiVO_4$/Au and FTO/WO_3/$BiVO_4$ electrodes under periodical visible light illuminations in N_2-bubbled 0.5M Na_2SO_4 aqueous solution. Scan rate was 50 mVs^{-1}. Electrodeposition time of Au nanoparticles was 60 s.

Figure 6. Nyquist plots for FTO/$BiVO_4$, FTO/WO_3/$BiVO_4$ and FTO/WO_3/$BiVO_4$/Au electrodes in N_2-bubbled 0.5M Na_2SO_4 aqueous solution under visible light illuminations. Electrodeposition

time of Au nanoparticles was 60 s. The inset shows equivalent circuit for the electrochemical system of water oxidation reaction.

Figure 7. (A) The photocurrent of FTO/WO_3/$BiVO_4$/Au electrode for water oxidation under visible light irradiation at 0.4 V (vs Ag/AgCl) are plotted as a function of the electrodeposition time for Au nanoparticles. (B) The charge transfer resistance of FTO/WO_3/$BiVO_4$/Au electrode measured by EIS method under visible light irradiation at 0.4 V (vs Ag/AgCl) is plotted as a function of the electrodeposition time for Au nanoparticles. .

Figure 8. The correlation between %IPCE and absorption spectrum of FTO/WO_3/$BiVO_4$/Au electrodes in N_2-bubbled 0.5M Na_2SO_4 aqueous solution under an applied potential of 0.4 V vs. Ag/AgCl.

Figure 9 (A) Energy diagram (at pH = 0) and (B) the particulate films of the hetero junction FTO/WO_3/$BiVO_4$/Au composite electrode showing the charge transfer process.

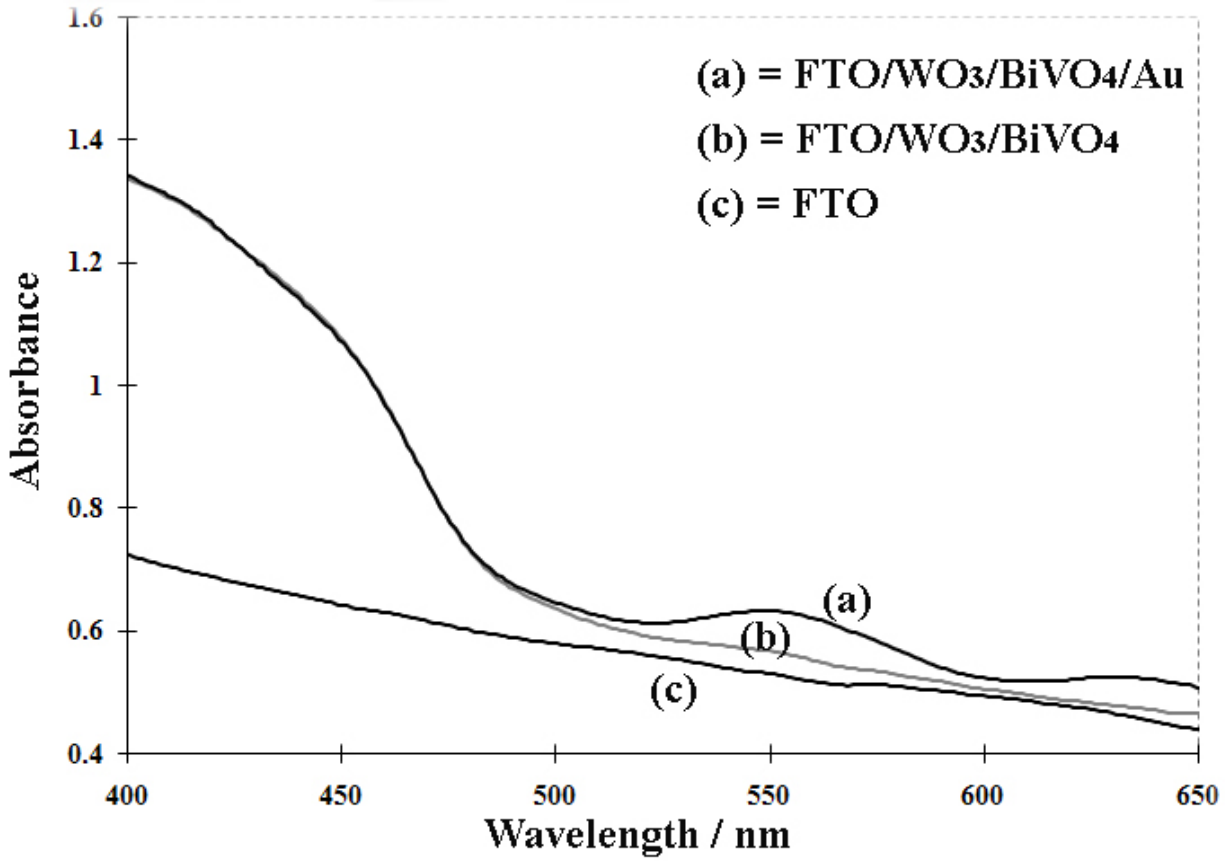

Figure 1. UV-Vis absorption spectra of (a) FTO/WO_3/$BiVO_4$/Au, (b) FTO/WO_3/$BiVO_4$ and (c) FTO electrodes. The interference by the film was corrected.

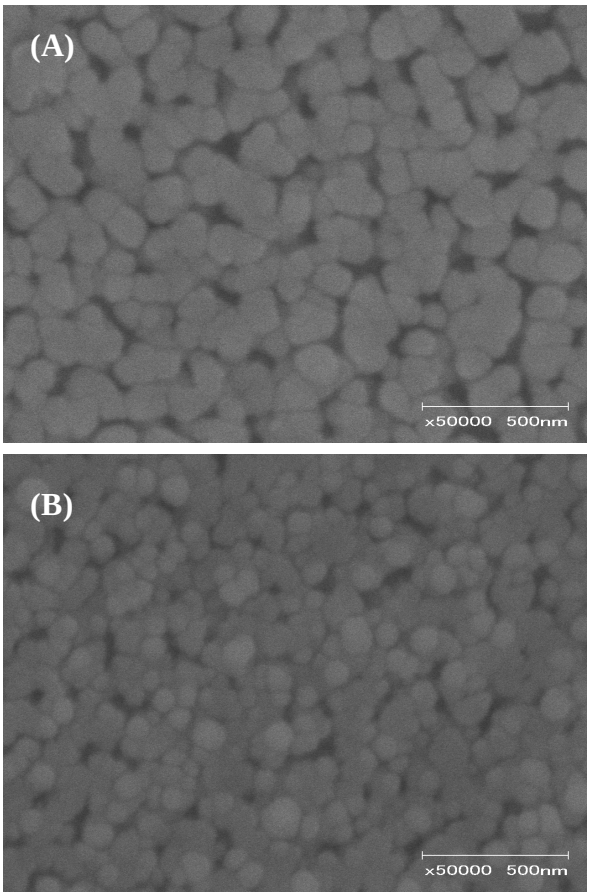

Figure 2. Scanning electron micrographs (SEM) at top view of (A) FTO/WO_3/$BiVO_4$, (B) FTO/WO_3/$BiVO_4$/Au

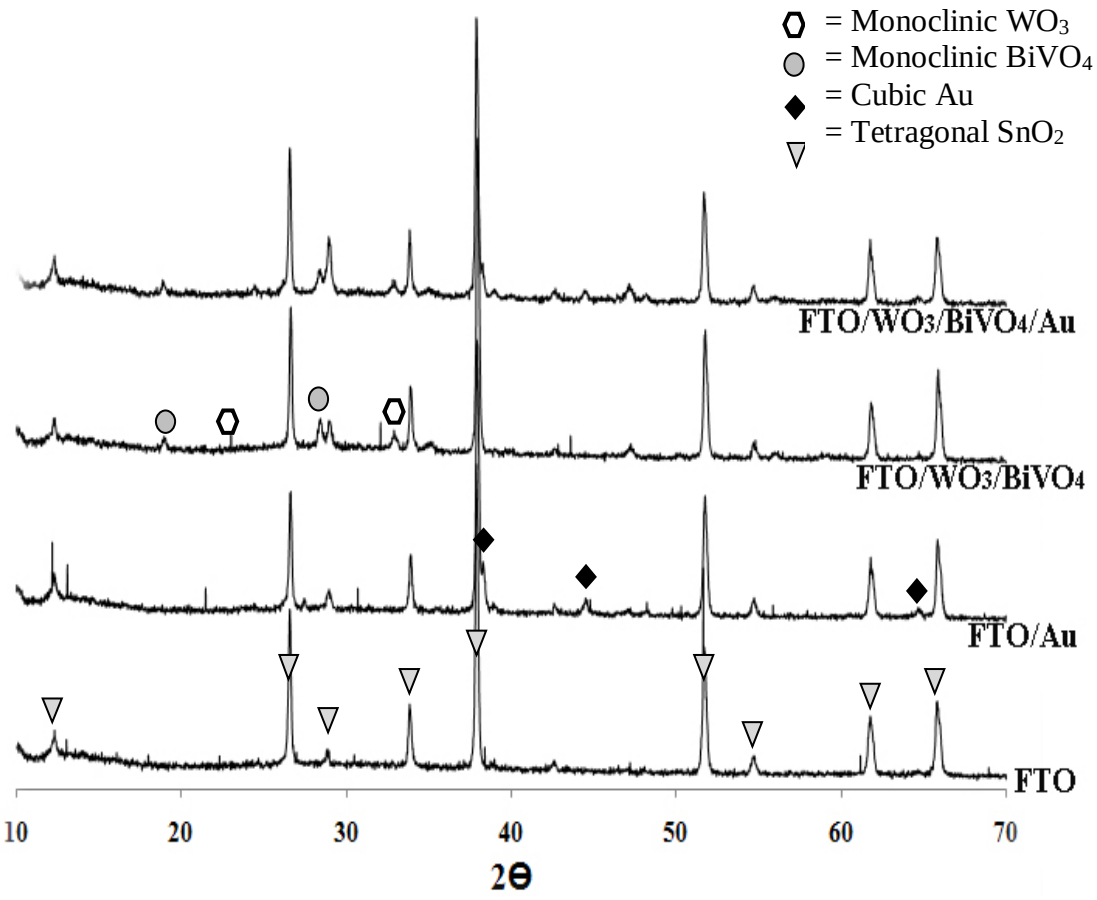

Figure 3. The XRD patterns for the FTO, FTO/Au, FTO/WO_3/$BiVO_4$, and FTO/WO_3/$BiVO_4$/Au electrodes which are calcined under the same condition at 550ºC.

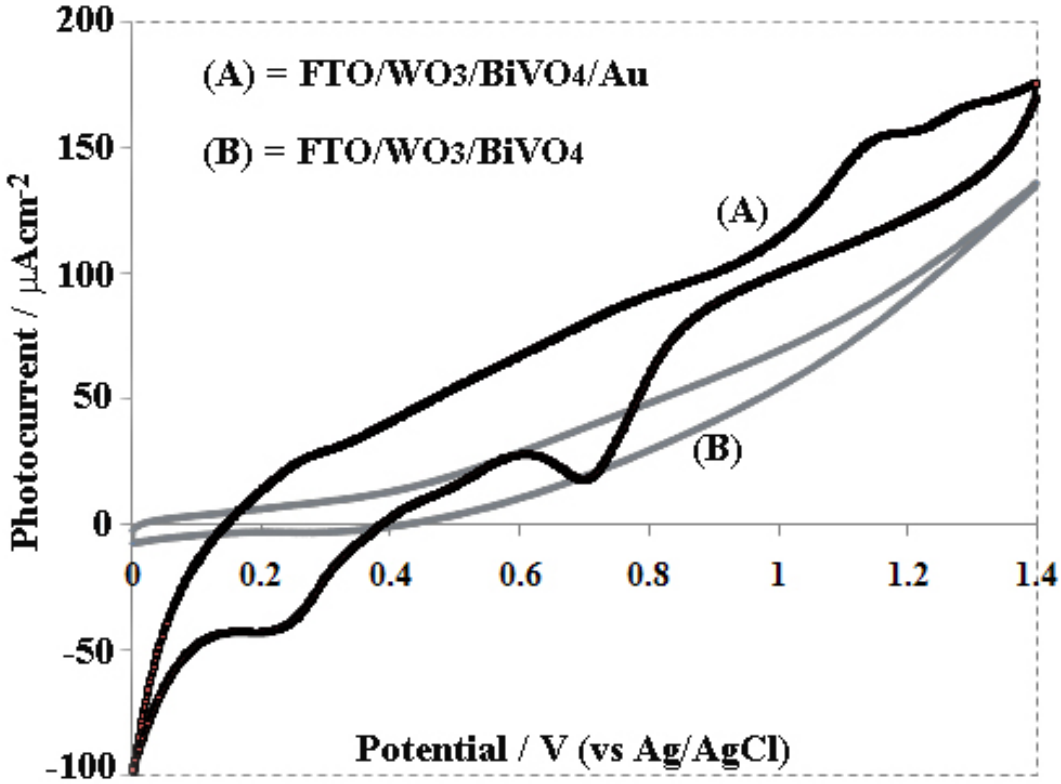

Figure 4. Comparison of cyclic voltammograms between FTO/WO_3/$BiVO_4$/Au and FTO/WO_3/$BiVO_4$ composite electrodes in 0.5 M Na_2SO_4 aqueous solution under the visible light illumination (> 420 nm). Scan rate was 50 mVs^{-1}. Electrolyte solution was deaerated by N_2 gas. Electrodeposition time of Au nanoparticles was 60 s.

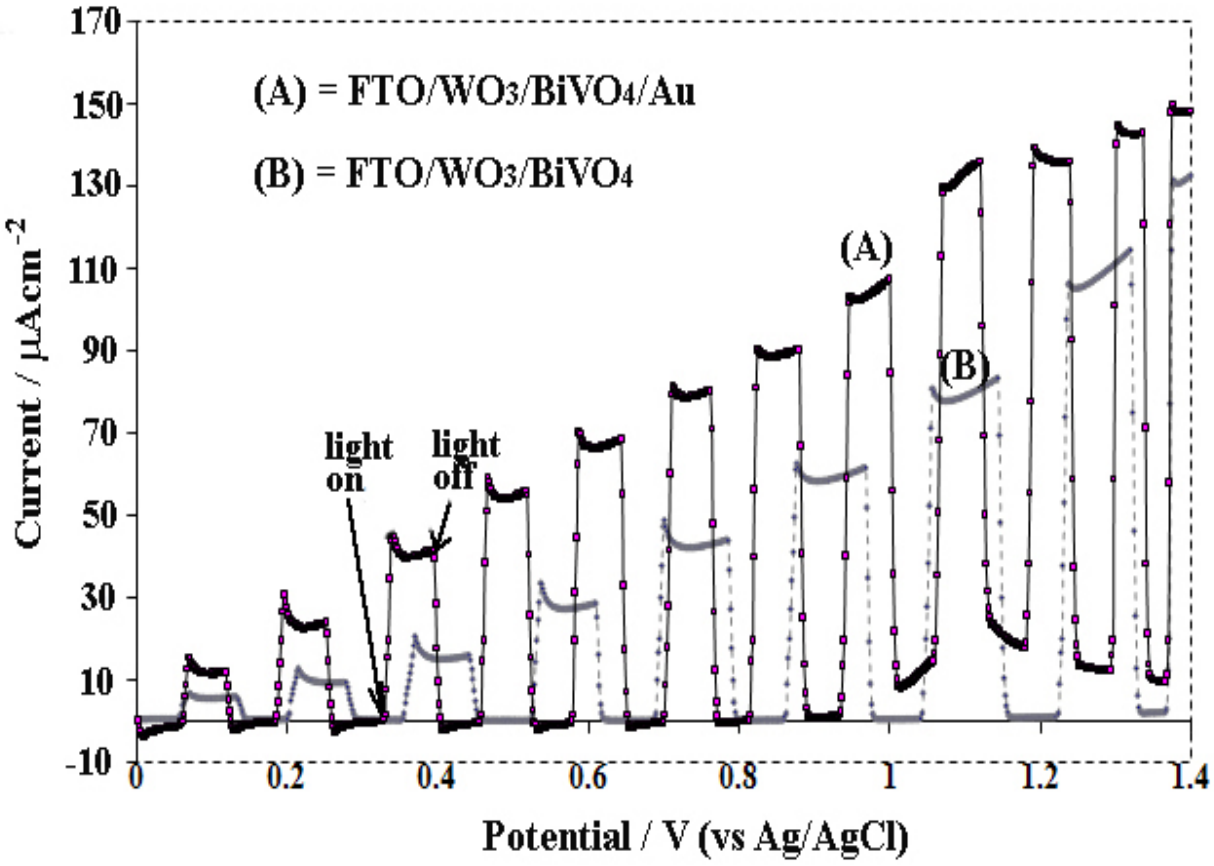

Figure 5. Linear scan voltammograms of $FTO/WO_3/BiVO_4/Au$ and $FTO/WO_3/BiVO_4$ electrodes under periodical visible light illuminations in N_2-bubbled 0.5M Na_2SO_4 aqueous solution. Scan rate was 50 mVs^{-1}. Electrodeposition time of Au nanoparticles was 60 s.

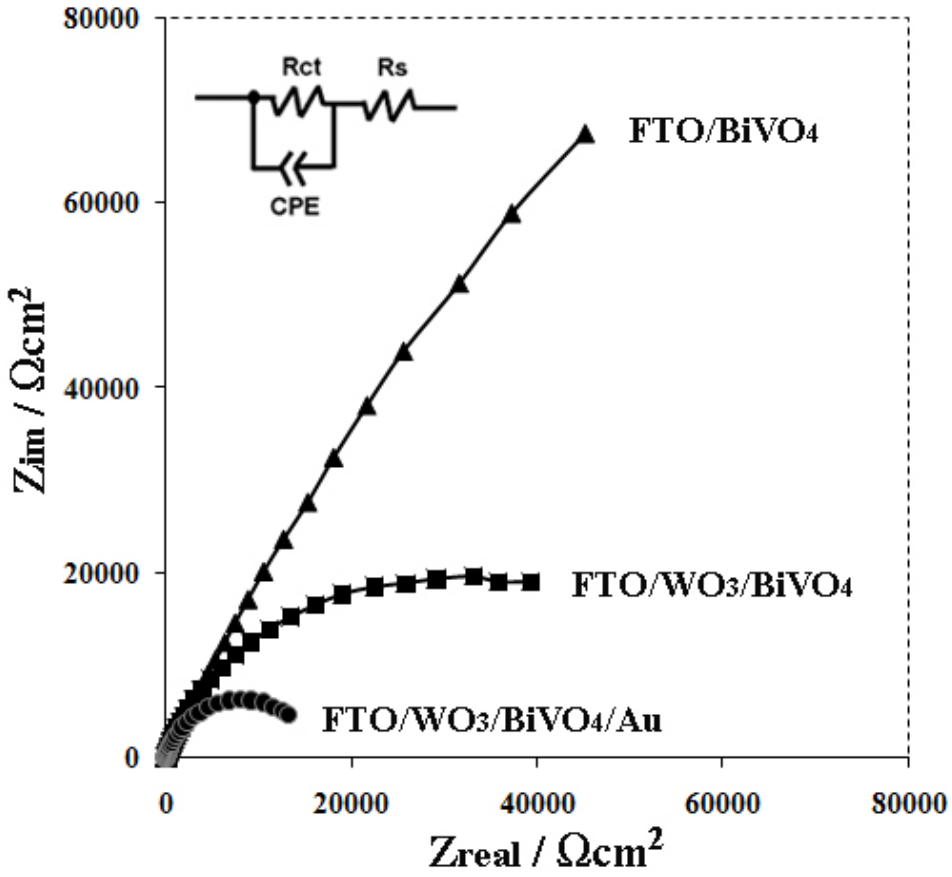

Figure 6. Nyquist plots for $FTO/BiVO_4$, $FTO/WO_3/BiVO_4$ and $FTO/WO_3/BiVO_4/Au$ electrodes in N_2-bubbled 0.5M Na_2SO_4 aqueous solution under visible light illuminations. Electrodeposition time of Au nanoparticles was 60 s. The inset shows equivalent circuit for the electrochemical system of water oxidation reaction.

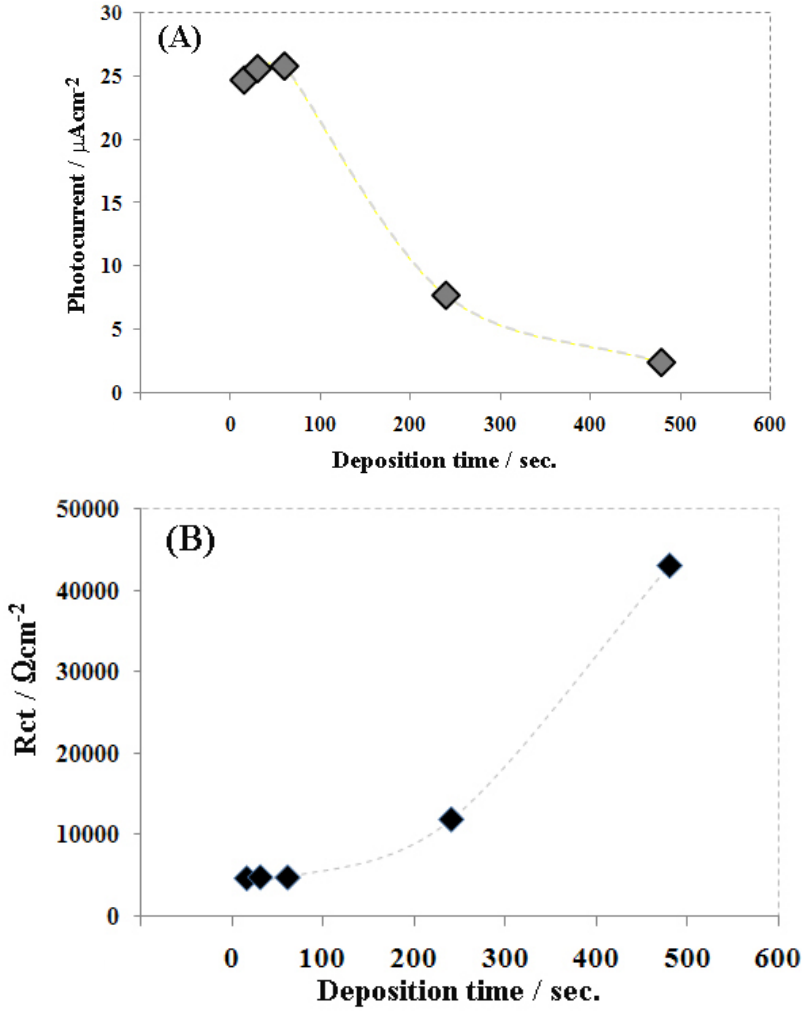

Figure 7. (A) The photocurrent of FTO/WO_3/$BiVO_4$/Au electrode for water oxidation under visible light irradiation at 0.4 V (vs Ag/AgCl) are plotted as a function of the electrodeposition time for Au nanoparticles. (B) The charge transfer resistance of FTO/WO_3/$BiVO_4$/Au electrode measured by EIS method under visible light irradiation at 0.4 V (vs Ag/AgCl) is plotted as a function of the electrodeposition time for Au nanoparticles.

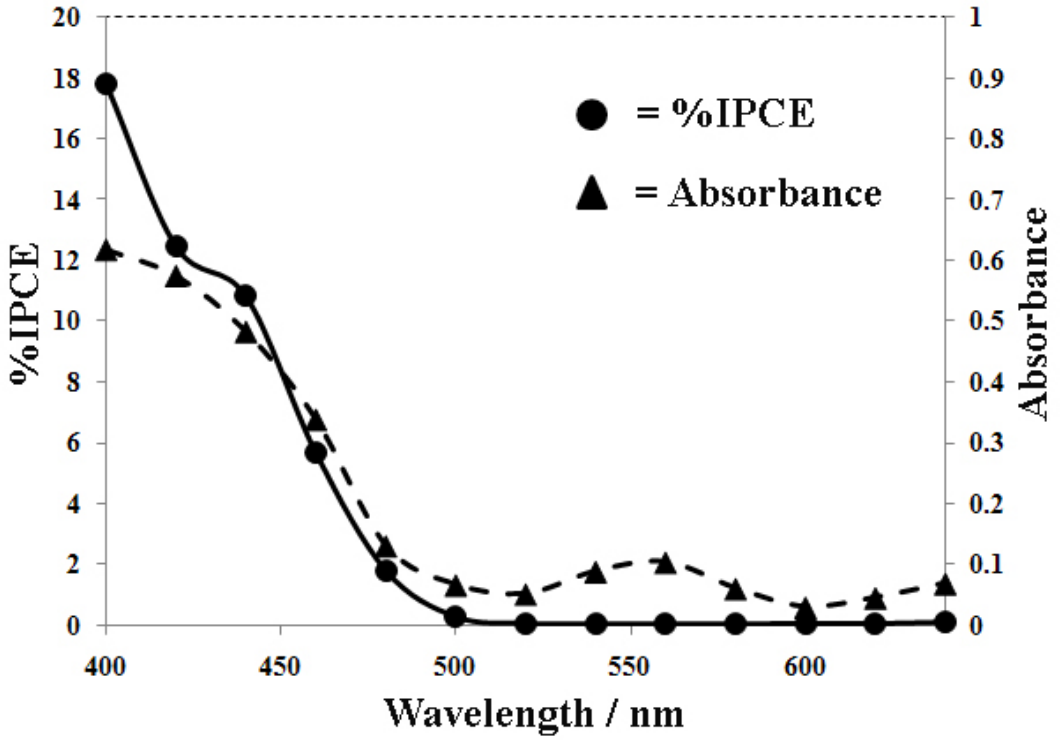

Figure 8. The correlation between %IPCE and absorption spectrum of FTO/WO_3/$BiVO_4$/Au electrodes in N_2-bubbled 0.5M Na_2SO_4 aqueous solution under an applied potential of 0.4 V vs. Ag/AgCl.

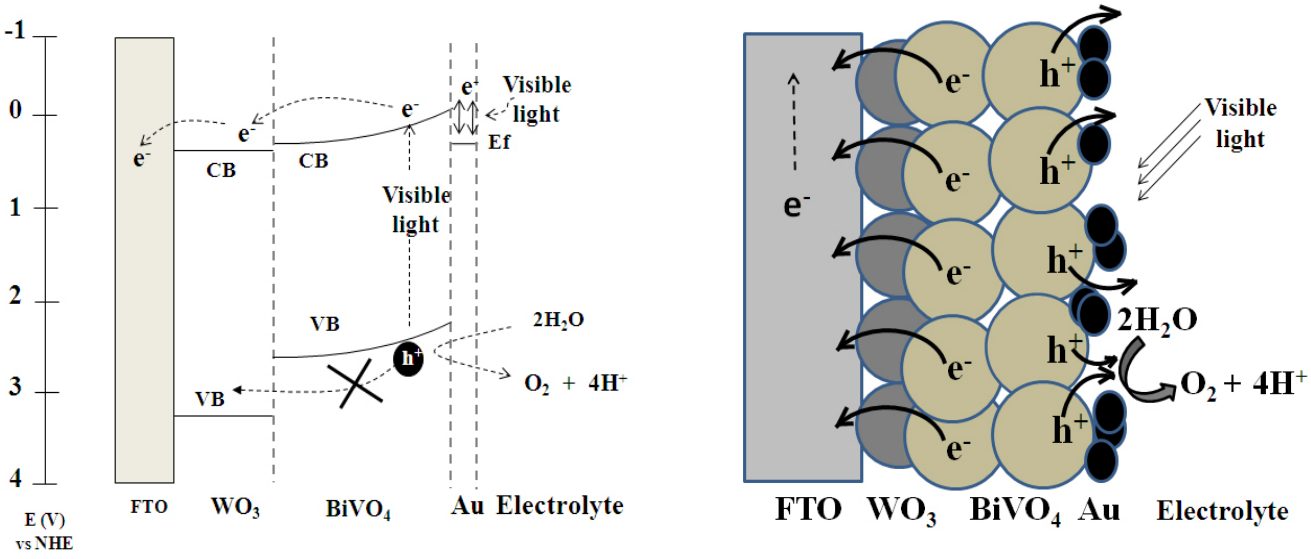

Figure 9 (A) Energy diagram (at pH = 0) and (B) the particulate films of the hetero junction FTO/WO_3/$BiVO_4$/Au composite electrode showing the charge transfer process.